Geophys J. R. astr. Soc. (1985) **82,** 105–123

The Backus–Gilbert approach to the three-dimensional structure in the upper mantle – I. Lateral variation of surface wave phase velocity with its error and resolution

Toshiro Tanimoto* *Seismological Laboratory, California Institute of Technology, Pasadena, California 91125, USA*

Accepted 1984 December 27. Received 1984 December 17; in original form 1984 September 19

Summary. The Backus–Gilbert method is applied to obtain the phase velocity variations on a sphere from the measured phase velocity. Narrow peak kernels, with radii of about 2000 km, are obtained for almost everywhere on the sphere. The phase velocity results are thus interpreted as an average within such regions. The most trouble comes from the antipodal peak in the resolution kernel. This is evaluated as contamination and is incorporated in the error estimation. The total error, which is a root mean square of contamination from the antipodal peak and statistical error estimated from the data covariance matrix, is about 1 per cent of the phase velocity in the average earth model, which is the Preliminary Reference Earth Model (PREM). However, there is about a factor of 2 variation of errors on the sphere. Maximum variations of phase velocity are about 3–4 per cent of the phase velocity in the average earth model, and thus there still remain anomalies which exceed estimated errors. The estimated errors correspond to one standard deviation under the assumptions of uncorrelated Gaussian distribution. For high confidence interval, they show that statistically significant anomalies are scarce for the current data set. Generally, Love-wave phase velocity maps show more resolved features than Rayleigh-wave maps and we can see, in high confidence maps, fast velocities in old oceans and old continents and slow velocities in tectonically active regions like the East Pacific Rise and various back-arc regions.

1 Introduction

The large number of digital seismograms obtained from two digital seismograph networks, IDA (International Deployment of Accelerometers) and GDSN (Global Digital Seismograph Network), enabled two groups of researchers, one at the California Institute of Technology (Nakanishi & Anderson 1984b; Nataf, Nakanishi & Anderson 1984) and the other at Harvard

*Present address: Geophysics Program AK-50, University of Washington, Seattle, Washington 98195, USA.

university (Woodhouse & Dziewonski 1984) to produce three-dimensional maps of velocity anomalies in the upper mantle. The two groups used essentially the same approach, i.e. they obtained an average phase velocity between source and receiver, expanded many such measurements into spherical harmonics and solved these phase velocity variations for the radial variations of seismic velocities. A difference is that Nakanishi & Anderson (1984b) and Nataf *et al.* (1984) solved the problem step by step, while Woodhouse & Dziewonski (1984) solved the entire problem simultaneously and iteratively; Nakanishi & Anderson (1984b) measured phase velocities using a conventional single-station method, while Woodhouse & Dziewonski (1984) obtained them by fitting waveforms in the time domain by using a new idea of shifting of sources. One should note that, although Woodhouse & Dziewonski (1984) used normal mode theory, their additional assumptions, especially the dropping of two out of the three terms in equation (44) in Woodhouse & Girnius (1982), makes their method almost equivalent to the surface wave approach. It is quite remarkable that the two groups produced similar results, since their data sets are quite different and are analysed independently.

There remain a few problems, however. For example, neither group has shown error bars in their results. Also how well the data can resolve fine details in the results is not yet understood. Because of the use of truncated spherical harmonics and the obvious existence of higher spherical harmonic components in the real Earth than the maximum truncation level, there may exist some aliasing effect in their solutions.

This paper is an attempt to answer these questions by the resolving power theory of Backus & Gilbert (1967, 1968, 1970). The principal aims of this paper are to understand errors and resolutions of the phase velocity variations. Recently, a similar approach was used by Whaler (1984) for a different problem: to detect fluid upwelling at the core–mantle boundary from geomagnetic data. Detection of azimuthal dependence of phase velocity as attempted by Tanimoto & Anderson (1984) is possible by a similar approach, but it will be discussed in a later paper.

The data set used here is almost equivalent to Nakanishi & Anderson (1984b), i.e. earthquakes in 1980, although some differences in the selections of earthquakes exist. The data set is equivalent to Tanimoto & Anderson (1985). Some of the results are in Tanimoto & Anderson (1985) without much discussion of the method. In the following, we discuss the method in detail and also present more complete results.

2 The Backus–Gilbert method: the first Dirichlet condition

We start from the following equation:

$$S_i = \int_s^R dl \cdot S(\theta, \phi) \tag{1}$$

where S_i is the ith datum of measured phase slowness and the right side of the equation denotes a line integral of the real phase slowness variation along the path. θ is colatitude, ϕ longitude, and the integral is from the source, s, to the receiver, R.

Next, we do the following transformation:

$$S_i = \int_s^R dl\, S(\theta, \phi),$$

$$= \int_s^R dl \sum_{l,m} A_{lm} \cdot Y_{lm}(\theta, \phi),$$

$$\equiv \sum_{l,m} A_{lm} \cdot P_{lm} \left(P_{lm} \equiv \int_s^R dl\, Y_{lm}(\theta, \phi) \right),$$

$$= \sum_{l,m} P_{lm} \cdot \int d\Omega \cdot Y_{lm}(\theta, \phi) \cdot S(\theta, \phi),$$

$$= \int d\Omega \left\{ \sum_{l,m} P_{lm} \cdot Y_{lm}(\theta, \phi) \right\} S(\theta, \phi),$$

$$\equiv \int d\Omega K_i(\theta, \phi) \cdot S(\theta, \phi), \tag{2}$$

where $Y_{lm}(\theta,\phi)$ is a spherical harmonic function. In essence, we transformed a line integral to an integral over a sphere by expanding a surface wave path into spherical harmonics. We used up to $l = m = 10$ to expand a path. Each path is given a certain width by this procedure. Assigned widths, however, are greater than the true widths. In order to represent widths faithfully, we must use much higher values for l and m. For example, at 200 s, the wavelength of surface waves is about 1000 km. Considering the asymptotic relation between the wavelength λ and the angular order of spherical harmonics l, $\lambda = 2\pi \times 6371/(l + 0.5)$, l must be as high as 40. What we would like to obtain in this paper, however, are the relatively low angular order components of lateral heterogeneity, approximately $l \leqslant 10$. Thus, although our procedure might produce some artificial smoothing, it is justified. Also rigorously, we must assign different widths to different frequencies, but we uniformly used $l = m = 10$ in this study.

We take a linear combination of (2) using all available data and obtain

$$\sum_i \alpha_i S_i = \int d\Omega \left\{ \sum_i \alpha_i K_i(\theta, \phi) \right\} \cdot S(\theta, \phi), \tag{3}$$

where $\alpha_i (i = 1, 2, \ldots)$ are coefficients to be determined by requiring the sum in { } in the right side of (3) become as close as possible to $\delta(\cos\theta - \cos\theta_0)\delta(\phi - \phi_0)$. We do this by minimizing

$$J = \alpha^t G \alpha + \tan\lambda \alpha^t V \alpha - 2\alpha^t K \tag{4}$$

where

$\alpha = (\alpha_1, \alpha_2, \ldots)^t$,

$G = (G_{ij}) = \int d\Omega K_i(\theta,\phi) \cdot K_j(\theta, \phi)$,

where $\tan\lambda$ is the trade-off parameter,

V is the covariance matrix of data

and

$K = (K_1(\theta_0, \phi_0), K_2(\theta_0, \phi_0), \ldots)^t$,

under the unimodular constraint

$$\sum_i \alpha_i \int K_i(\theta, \phi)\, d\Omega = 1.$$

This criterion is called the first Dirichlet condition.

Backus & Gilbert (1968) showed in their one-dimensional problem, i.e. the inversion of modal attenuation Q^{-1} for the radial distribution of intrinsic $Q^{-1}(r)$, that this criterion produces a narrow peak but at the same time fairly large sidelobes. In our case, as shown in the following sections, the method produces very satisfactory resolving kernels.

Another reason we used this criterion is that evaluations of matrix elements (G_{ij}) in (4) become almost analytical because we keep the spherical harmonic coefficients of paths $K_i(\theta, \phi)$ ($i = 1, 2, \ldots$). Any method that requires the numerical evaluation of two-dimensional integral in G_{ij} is too costly, since this integral has to be evaluated $n(n+1)/2$ times where n is the number of data.

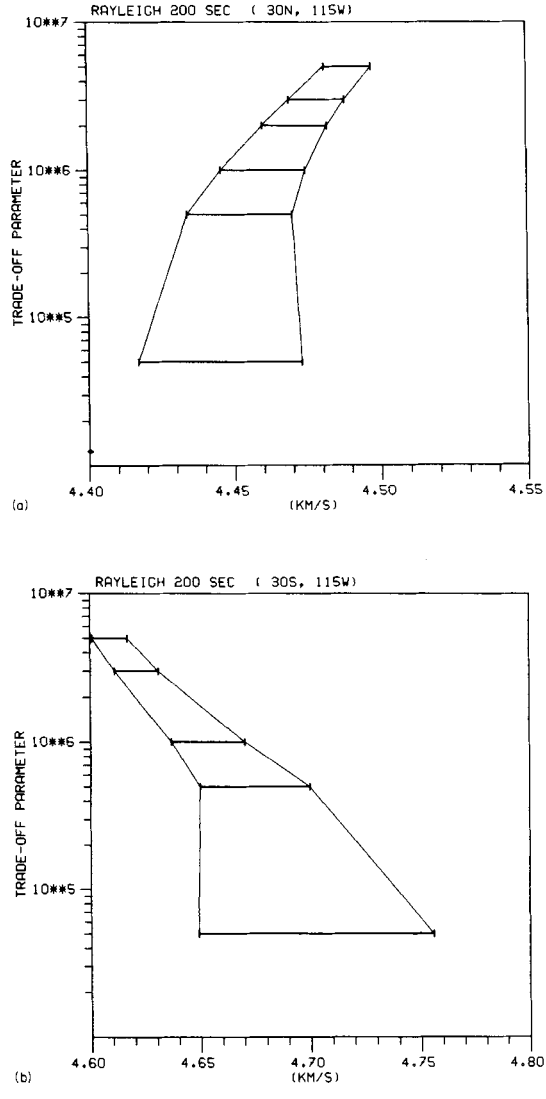

Figure 1. (a) The trade-off parameter versus estimated phase velocity bounds at (30° N, 115° W). As the trade-off parameter is increased, velocity bounds become tight. Note the systematic shift that occurs for the trade-off parameter greater than about 5×10^5. (b) Same as (a) except for a different location (30° S, 115° W).

Whaler & Gubbins (1981) studied a slightly different problem, i.e. to obtain spherical harmonic coefficients from observed values on a sphere by the Backus–Gilbert method and vice versa. They showed that another criterion, which has a weight $\frac{1}{2}\sin^2\psi$, where ψ is the distance between (θ, ϕ) and (θ_0, ϕ_0) in an integral like the other one in G_{ij}, allows analytical evaluation. This can be applied in our case, too, although we also have to transform the coordinate for each target location (θ_0, ϕ_0) and this clearly requires more computation time. Whaler (1984) also states a similar problem. We will report the comparisons of these criterions in a separate paper. The following results are obtained solely by the first Dirichlet condition.

3 Selection of trade-off parameter

First of all, we must select a trade-off parameter for the available data. We have approximately 600 paths for Rayleigh waves and 400 paths for Love waves at each frequency. We constructed graphs of trade-off parameter versus phase velocity bounds at various locations on the globe. Fig. 1(a, b) shows examples at (30°N, 115°W) near California and at (30°S, 115°S) near the East Pacific Rise, respectively. As pointed out by Gilbert (1971), to make such trade-off graphs, much computation time is saved by first decomposing G to $U\Lambda U^{\mathrm{T}}$, where U is an orthogonal matrix and Λ a diagonal matrix. Both figures clearly show a well-known trend, that is as we increase the trade-off parameter, we obtain smaller velocity bounds. At the same time, resolution kernels deviate further away from delta functions.

We also notice a systematic deviation of estimated phase velocity bounds for the trade-off parameter greater than about 5×10^5 or 10^6. This effect is caused mainly by antipodal peaks. Fig. 2(a, b) shows the shapes of resolution kernels for the trade-off parameters 5×10^4, 5×10^5 and 5×10^6 from top to bottom. Fig. 2(a, b) gives the results of the same locations with Figs 1(a) and 1(b) respectively. In both Figs 2(a) and 2(b), the amplitudes of sidelobes increase as the trade-off parameter is increased, but the effect is most significant at the antipodes. Amplitudes of oscillations away from (θ_0, ϕ_0) and its antipode are about 5 per cent of the peak at (θ_0, ϕ_0), while the peak at the antipode can become as large as 25 per cent for some target locations (θ_0, ϕ_0), e.g. $\tan\lambda = 5 \times 10^6$ in Fig. 2(b). In the present data set, we found empirically that velocity bounds start deviating systematically when the antipodal peak exceeds 20 per cent.

These observations give us a criterion to choose the trade-off parameter. Obviously, we want the velocity bounds as small as possible, while avoiding systematic deviation of phase velocity estimation. The optimal range of the trade-off parameter in the present problem is between 5×10^5 and 10^6. We selected $\tan\lambda = 10^6$ and used it uniformly for all locations on the globe. All results in the following sections are for $\tan\lambda = 10^6$.

4 Contamination and total errors

Error bars shown in Fig. 1(a, b) represent values obtained from $\alpha^{\mathrm{t}} V \alpha$, under the assumption that measurement errors are uncorrelated. Shapes of resolution kernels in Fig. 2(a, b) show, however, that estimated results contain a fairly large contribution from the antipodes. We evaluate this effect, which we call 'contamination' in this paper (Masters 1979), and incorporate it in the error estimation.

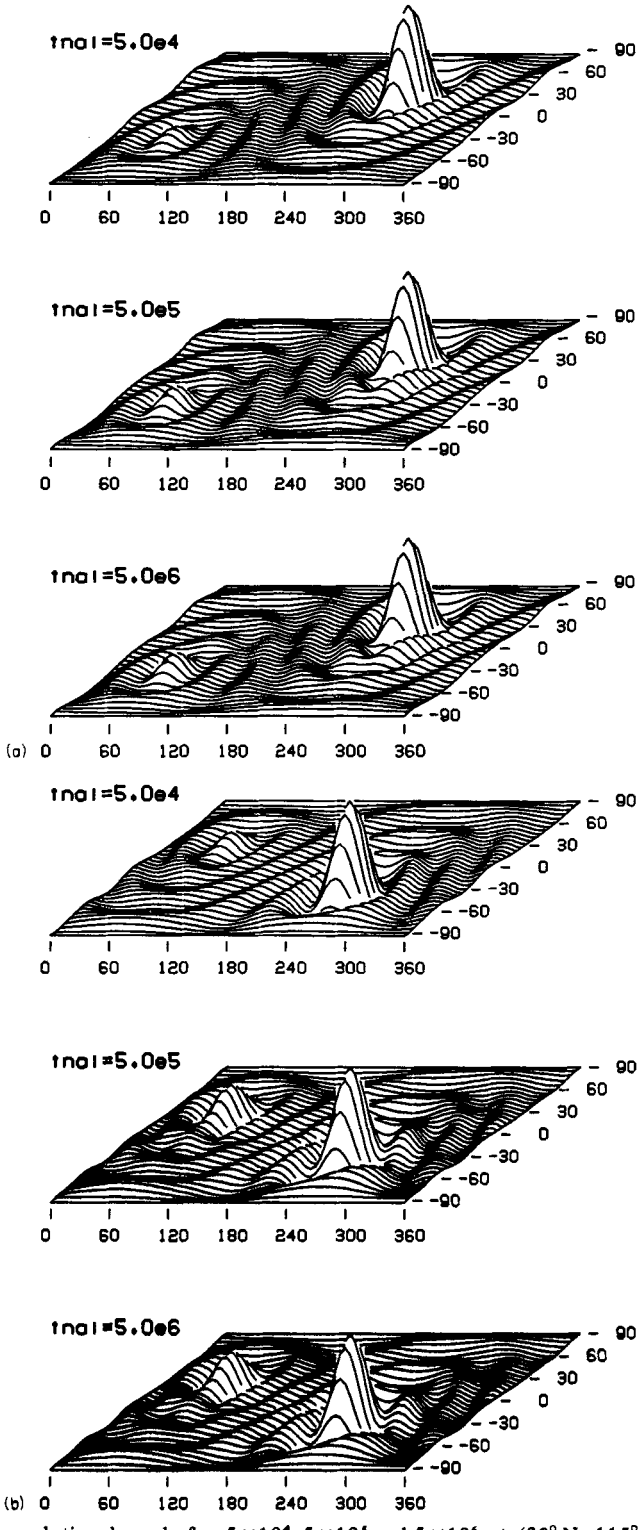

Figure 2. (a) The resolution kernels for 5×10^4, 5×10^5 and 5×10^6 at (30° N, 115° W). (b) Same as (a) except for (30° S, 115° W).

We proceed in the following way: the estimated phase slowness at (θ_0, ϕ_0) is expressed by

$$\bar{S}(\theta_0, \phi_0) = \int d\Omega \cdot \bar{K}(\theta, \phi) \cdot S(\theta, \phi),$$

$$= \int_{\text{antipode}} d\Omega \bar{K} \cdot S + \int_{\text{other}} d\Omega \bar{K} \cdot S,$$

where the first term is the contamination and $\bar{K}(\theta, \phi)$ the resolution kernel for (θ_0, ϕ_0). We evaluate this by

$$\left| \int_{\text{antipode}} \bar{K} \cdot S \, d\Omega \right| \leq \int_{\text{antipode}} |\bar{K}| \cdot |S| \, d\Omega$$

$$\leq |S_{\max}| \cdot \int_{\text{antipode}} |\bar{K}| \, d\Omega$$

$$\equiv C$$

where $S_{\max}$ is the maximum value of $S(\theta, \phi)$. Knowledge of this value is required to evaluate C. We assumed 5 per cent of phase slowness in the reference earth model. The results in the next section show less variation than this value and the use of 5 per cent seems to be safe.

In evaluating the integral

$$\int_{\text{antipode}} |\bar{K}| \, d\Omega,$$

we integrated a region of 20° radius around the antipode. In order to do this, instead of using the original spherical harmonic coefficients, we transformed coordinate frames to the one in which the antipode coincides with the south pole and integrated the region around the south pole. This made it easier to code the program, reduced computation time and also helped to confirm that the antipodal peak is confined within an area of 20° radius.

Let $\epsilon^2 = \alpha^t V \alpha$. We defined the total error, ϵ_{tot}, by combining ϵ^2 and c as

$$\epsilon_{\text{tot}} = \sqrt{\epsilon^2 + c^2}.$$

In the following, we show the results of the total error, ϵ_{tot}, instead of ϵ^2.

5 Results

5.1 RESOLUTION KERNELS

First, we show the results of resolution kernels at various locations in the Earth. All kernels are for Rayleigh waves at 200 s and for $\tan \lambda = 10^6$. Similar kernels can be constructed at different frequencies and also for Love waves.

Fig. 3(a–j) shows the shapes of kernels in a contoured map at the top and in a three-dimensional map at the bottom. In the contoured map, the maximum value at the target (θ_0, ϕ_0) is normalized as 1 and the lines corresponding to 0.8, 0.6, 0.4, 0.2 and 0 are drawn. Positive regions are shaded.

Quite localized peaks with radii of about 2000 km are produced for all maps. Some regions, e.g. Figs 3(c) and 3(h), seem to have broader peaks, but this is because of the way we plot these maps and their proximity to the polar region.

Antipodal peaks vary in amplitude from place to place. For well sampled regions, e.g. Japan (Fig. 3d) or Australia (Fig. 3f), antipodal peaks are less than 20 per cent, while for poorly sampled regions they exceed 20 per cent. Note, however, that even for poorly covered regions, we have almost about 40 surface wave rays passing nearby (Tanimoto & Anderson 1984, fig. 1), a number which is often considered sufficient in many other studies. Amplitudes of sidelobes, other than the antipodal peaks, are also correlated well with sampling of paths. This is clearly illustrated by comparing Figs 3(f) and 3(g).

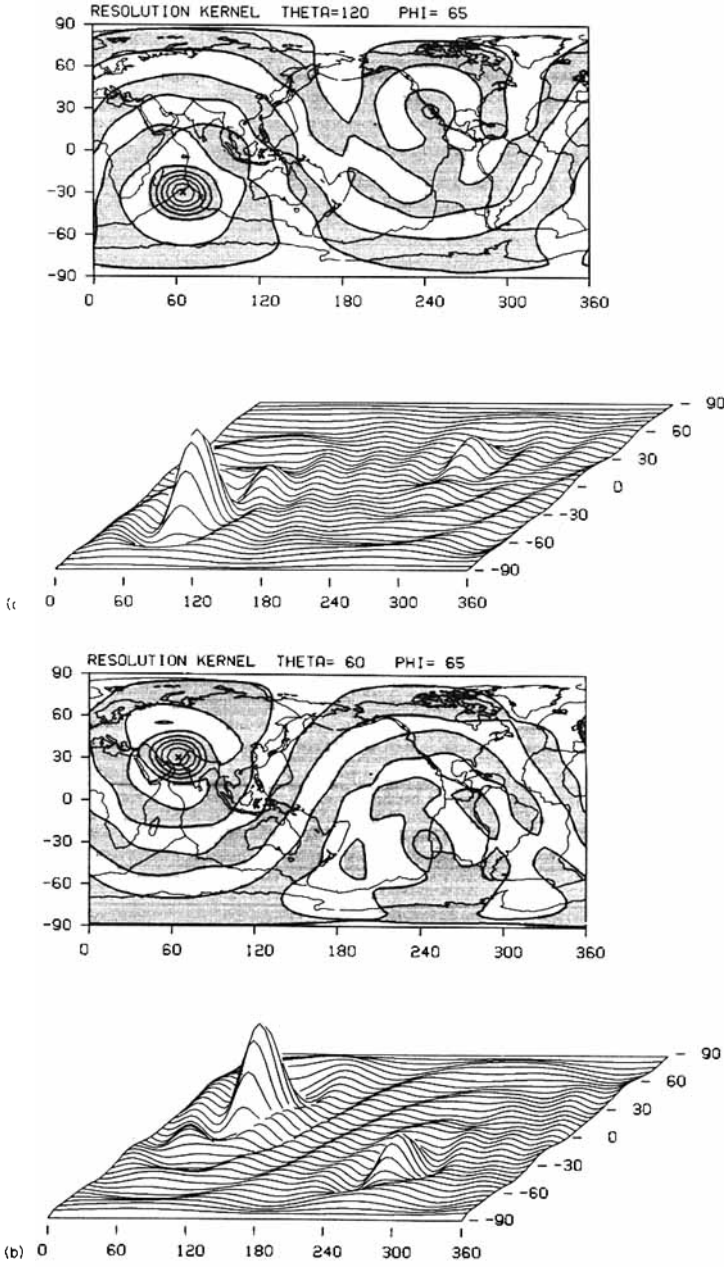

Figure 3. (a–j) Resolution kernels for various locations. The trade-off parameter is 10^6.

5.2 PHASE VELOCITY AND ERROR MAPS

We constructed a resolution kernel at each 5° interval both in latitude and longitude and obtained a phase velocity variation map and total error map for Love and Rayleigh waves at different frequencies.

Fig. 4(a) gives the result of Love waves at 200 s. In the top figure, we present the phase

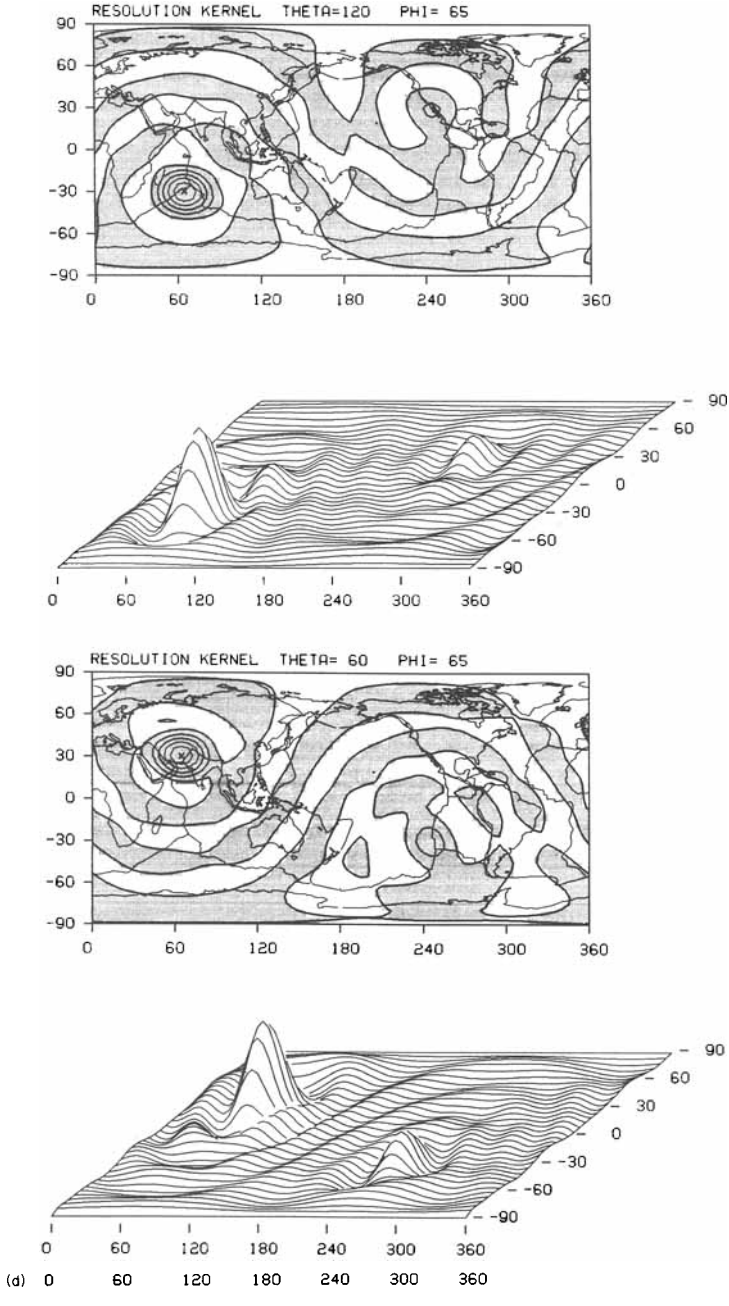

Figure 3 – *continued*

velocity variation at each 1 per cent contour interval. These values are referenced to the phase velocities of the Preliminary Reference Earth Model (Dziewonski & Anderson 1981), that is a quite accurate zeroth-order spherically symmetric earth model for periods longer than about 150 s. Shaded regions denote a positive or fast velocity region. The bottom figure shows the variation of errors. In this figure, contours are drawn at each 0.2 per cent interval and the regions of more than 1 per cent error are shaded. Thus, non-shaded regions in this

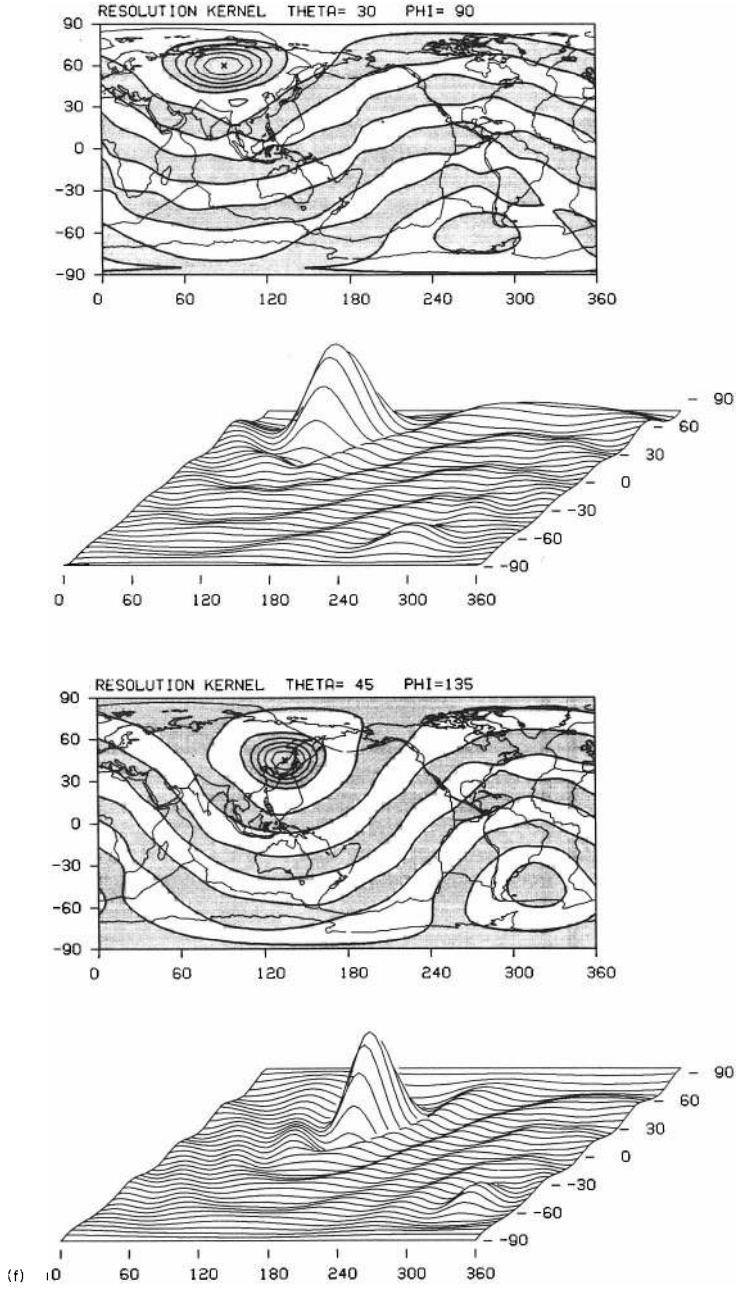

Figure 3 – *continued*

figure have errors between 0.8 and 1.0 per cent, while the maximum error regions have a little over 1.4 per cent error and are found near the East Pacific Rise and northern Indian Ocean. It is clear from this error map that any velocity anomalies with less than about 1 per cent in the phase velocity variation map are not yet resolved.

Fig. 4(b) gives the results for Rayleigh waves at 200 s. The phase velocity map shows less variation than that of Love waves, which is probably because Rayleigh waves penetrate much

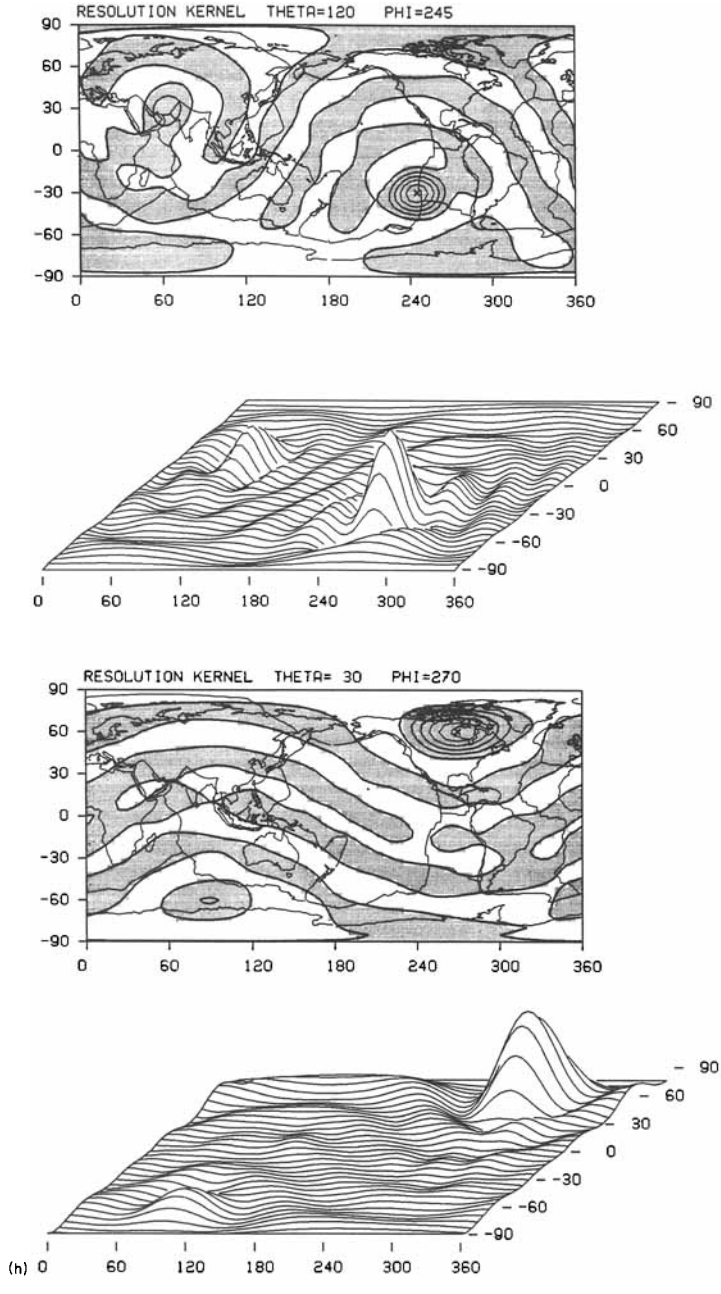

Figure 3 – *continued*

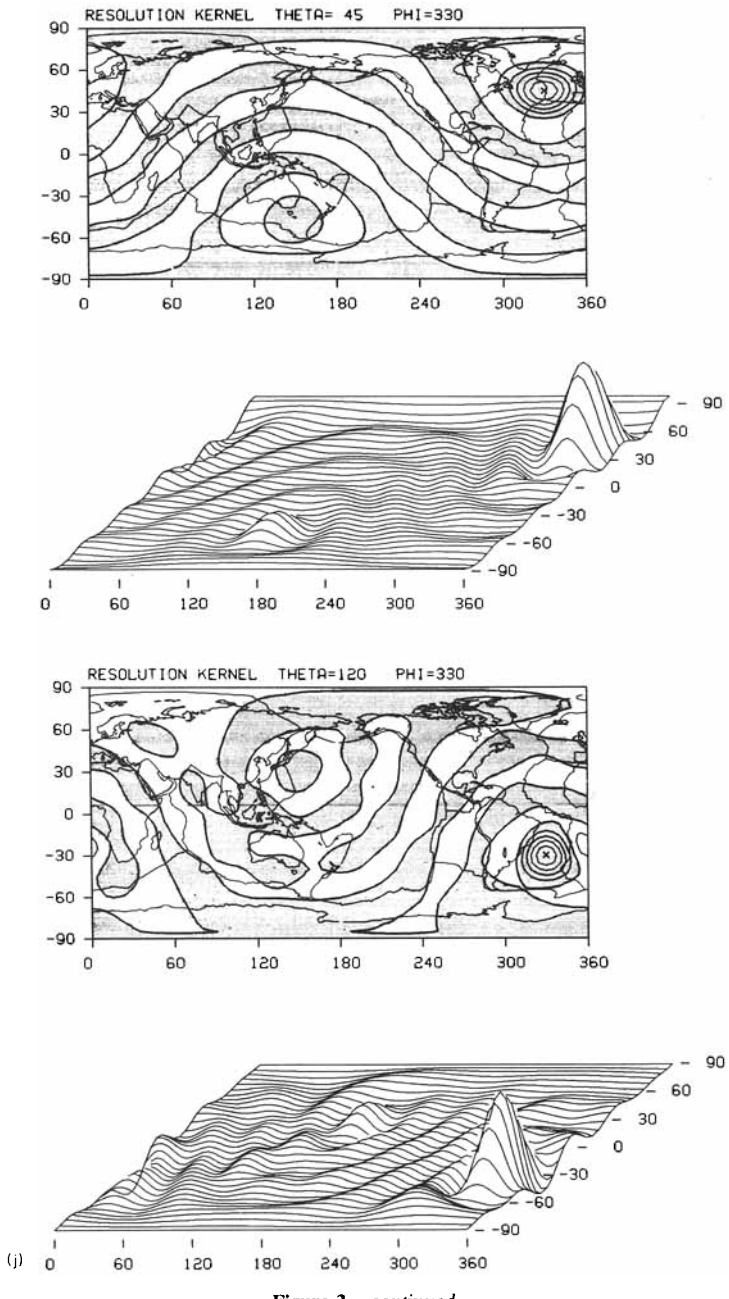

(j)

Figure 3 – *continued*

deeper to the more homogeneous depth than do Love waves. The error map also shows systematically smaller values. In this case, error varies from about 0.6 to 1.2 per cent. This is because we have more Rayleigh-wave data (about 600) than Love-wave data (about 400). However, a factor of about 2 variation on the globe and the locations of the maximum errors, i.e. near the East Pacific Rise and in the northern Indian Ocean, are the same. These features are the same with other frequencies.

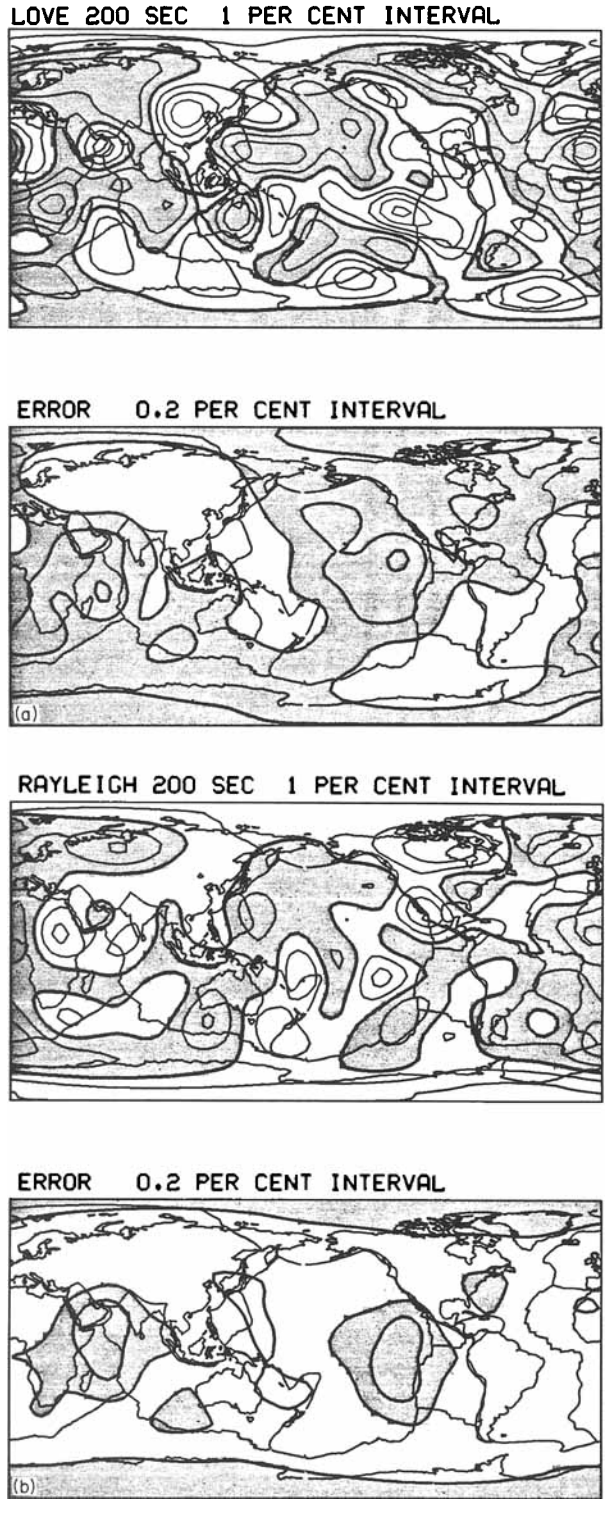

Figure 4. (a) Phase velocity variation map and error map for Love waves at 200 s. (b) Same as (a) except for Rayleigh waves.

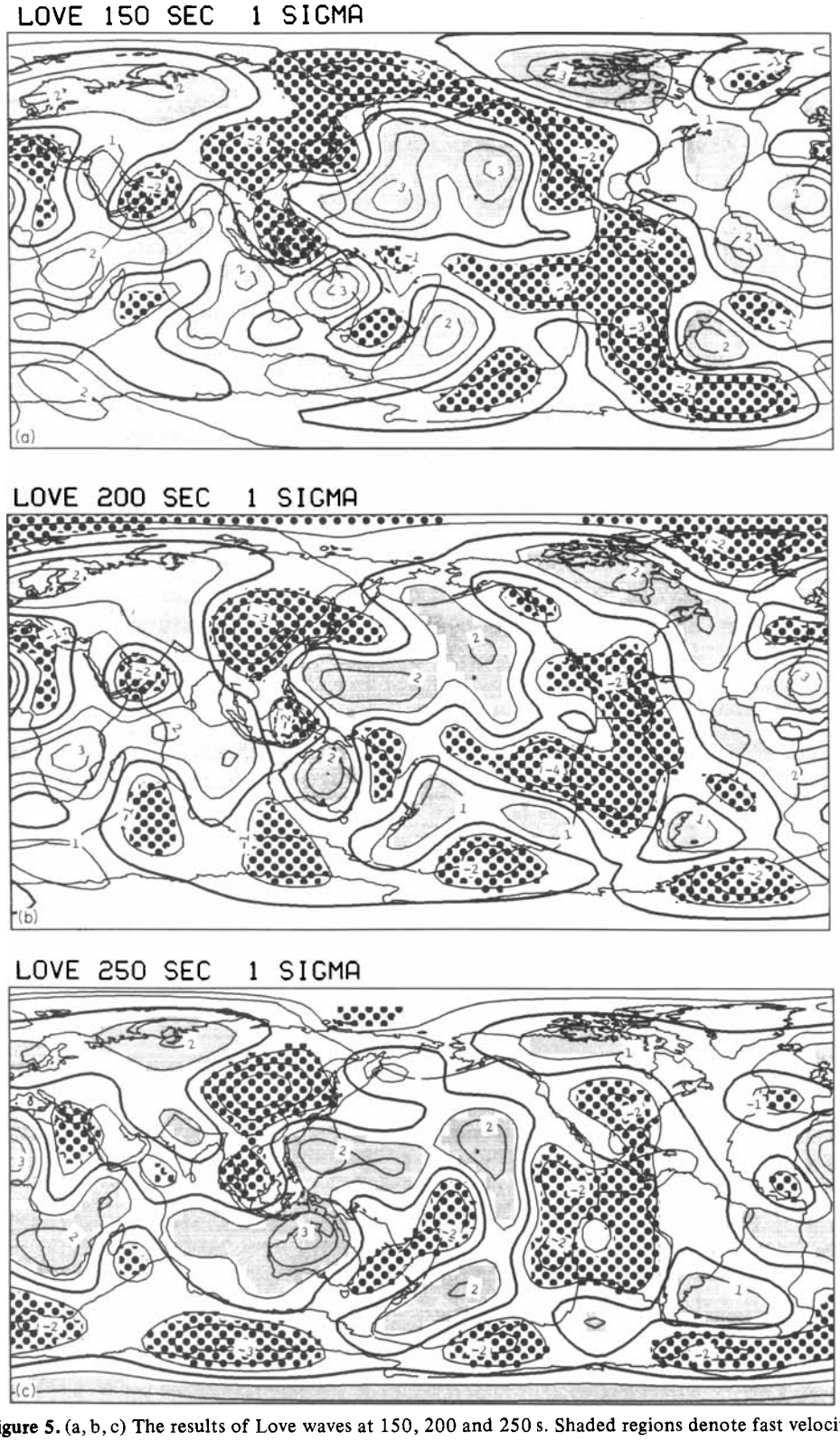

Figure 5. (a, b, c) The results of Love waves at 150, 200 and 250 s. Shaded regions denote fast velocity and dotted regions denote slow; both exceed the estimated errors.

5.3 COMBINED MAPS: 1σ CASE

For convenience, we combined information in a phase velocity map and an error map. Fig 5(a, b, c) shows the results of Love waves at periods of 150, 200 and 250 s. Contours are drawn in the same way with the top figures in Fig. 4(a, b). Shaded regions are regions with fast velocity anomalies which are larger than estimated errors. For slow velocity regions, we used a dotted pattern. Regions with values less than estimated errors are not filled with any patterns. Because estimated errors are about 1 per cent, patterned regions with shades and dots almost correspond to anomalies larger than 1 per cent. Clearly, we cannot believe the shapes of zero lines or the shapes of positive or negative regions. But we also see large areas of significantly fast or slow velocity regions on the globe.

These areas are smaller for Rayleigh waves than for Love waves and are shown in Fig. 6(a, b, c). Although Rayleigh-wave phase velocity errors are smaller than Love-wave phase velocity errors, the true variation of phase velocity is much less for Rayleigh waves (Fig. 4a, b). This is probably the reason for less significant regions of Rayleigh waves.

5.4 COMBINED MAPS: 2σ CASE

In Section 5.3, we used the estimated total error to specify significantly fast or slow regions. However, under the assumptions that all errors are independent and Gaussian, the estimated errors are one standard deviation. This corresponds to only 68 per cent of confidence interval. Thus, we produced higher confidence interval maps. We doubled the estimated errors and showed the anomalies which exceed these ranges in Fig. 7(a, b, c) for Love waves and in Fig. 8(a, b, c) for Rayleigh waves. They correspond to about 95 per cent confidence interval.

Regions having anomalies larger than the estimated errors are reduced considerably in these figures. More importantly, however, we can still see some anomalies. In the Love-wave maps (Fig. 7a, b, c), slow velocities along the East Pacific Rise and back-arc regions are still apparent. At 150 s, the slow anomaly near Saudi Arabia remains. Fast anomalies in old continents like Canada, north-western Eurasia and Australia and also in old ocean like the western Pacific are observed. In the Rayleigh-wave maps (Fig. 8a, b, c), western Eurasia remains fast and western Australia shows fast velocities for shorter periods. In our results, Canada tends to have slow Rayleigh-wave velocities and the anomaly remains significant even for the 2σ error map. This is consistent with Nakanishi & Anderson (1984b), which is not surprising since we used almost the same data set. The results of Woodhouse & Dziewonski (1984), however, exhibit fast velocities in this region. At longer periods, however, their results also show slow velocities.

Another region of interest is the fast velocity anomaly in the southern Atlantic Ocean. This is the region postulated to be continental roots or subducted old lithosphere (Nakanishi & Anderson 1984a).

6 Conclusions

We summarize the main conclusions of the present paper as follows:

(1) From about 400 (Love) and 600 (Raleigh) phase velocity measurements, we can construct a fairly sharp resolution kernel, which is localized within an area of 2000 km radius. Thus, phase velocity variations should be interpreted as an average of such a region.

(2) The antipodal peak, in the case of optimal or near optimal choice of the trade-off parameter, can be as large as 20 per cent of the peak at the target location (θ_0, ϕ_0).

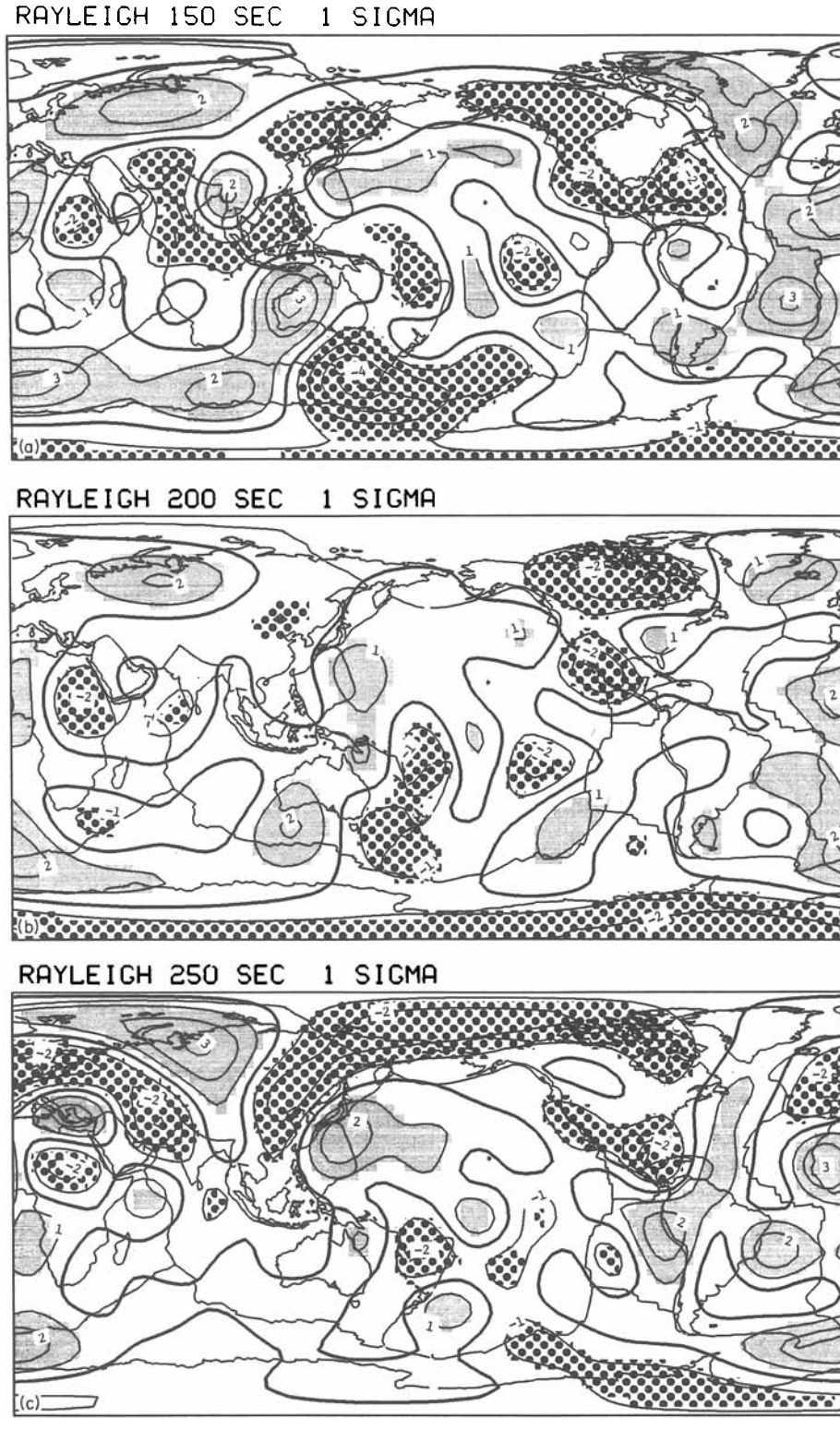

Figure 6. (a, b, c) Same as Fig. 5(a, b, c), except for Rayleigh waves.

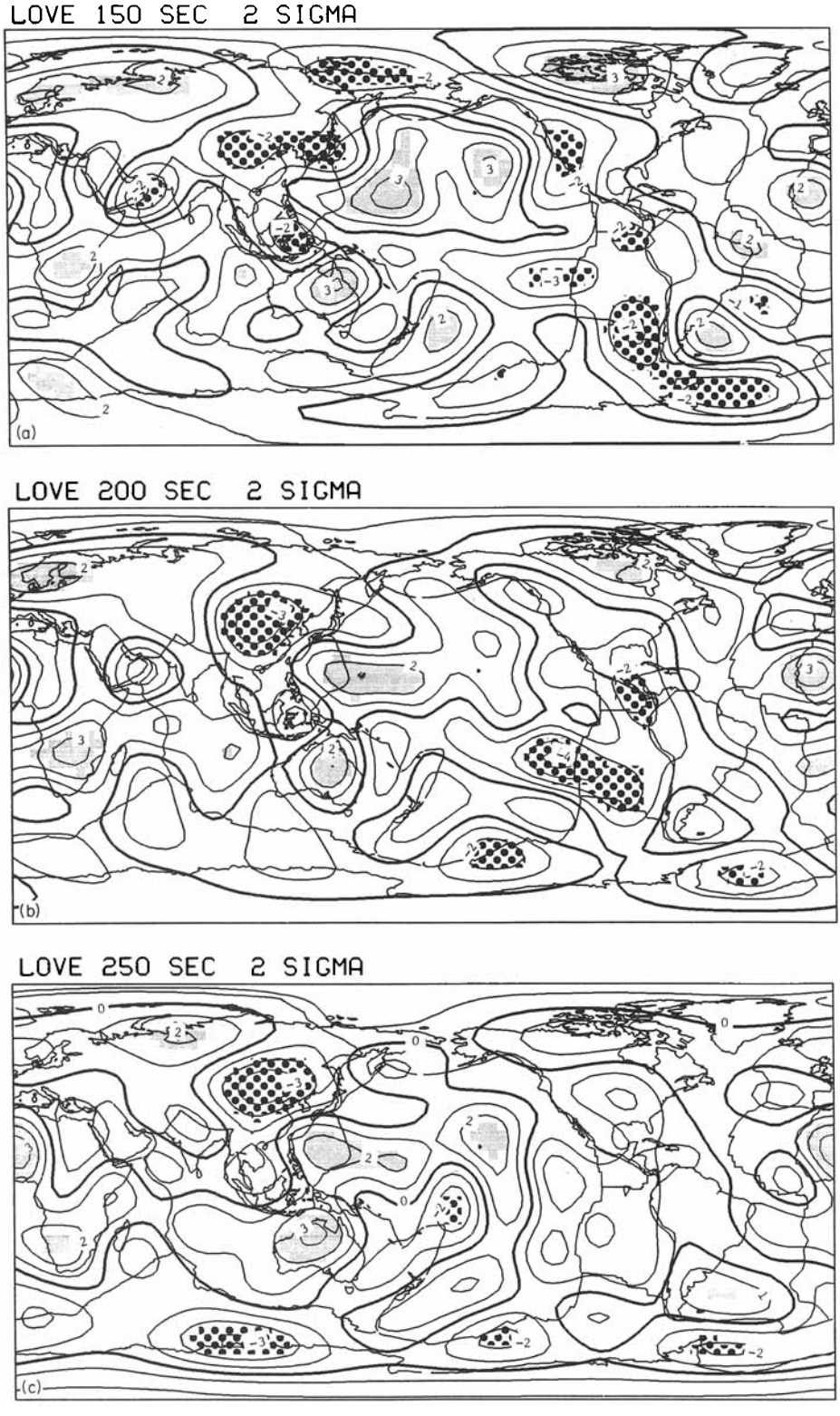

Figure 7. (a, b, c) The Love wave results of high confidence interval. Estimated errors are doubled and the regions whose anomalies exceed these values are shown by shades and dots.

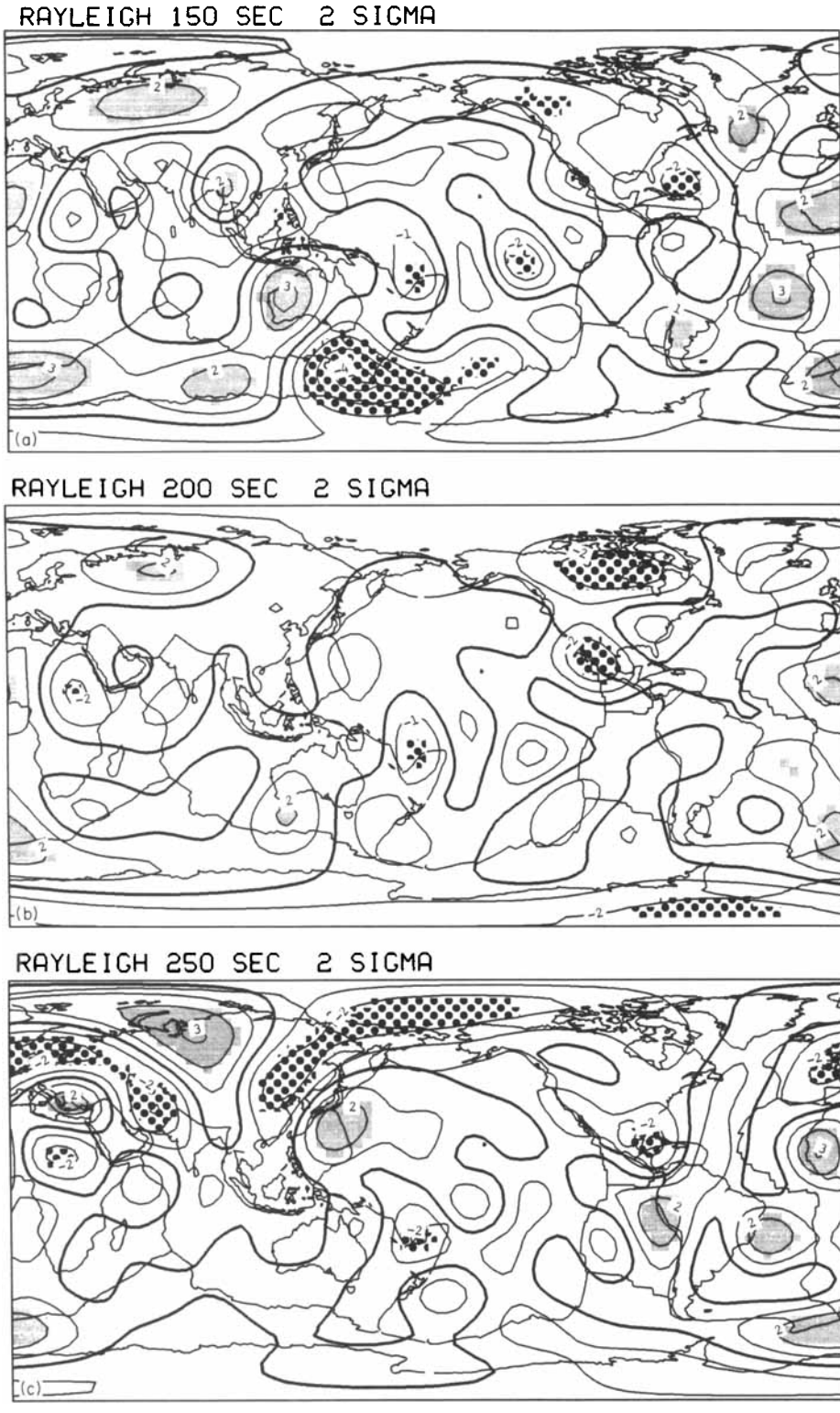

Figure 8. (a, b, c) Same as Fig. 7 (a, b, c) except for Rayleigh waves.

(3) Contamination or bias from this effect cannot be ignored. The combined effect of this contribution and the statistical error becomes about 1 per cent of the phase velocity in the averaged earth.

(4) Maximum phase velocity variations are about 3–4 per cent. Thus, we still see anomalies which are larger than estimated errors.

(5) For the high confidence case, the resolvable anomalous regions become scarce.

Acknowledgments

I thank Professor Don L. Anderson for his encouragement during the course of this study. This research was supported by National Science Foundation grant number EAR-8317623. Contribution number 4041, Division of Geological and Planetary Sciences, California Institute of Technology.

References

Backus, G. E. & Gilbert, F., 1967. Numerical application of a formalism for geophysical inverse problems, *Geophys. J. R. astr. Soc.*, **13**, 247–276.

Backus, G. E. & Gilbert, F., 1968. The resolving power of gross Earth data, *Geophys. J. R. astr. Soc.*, **16**, 169–205.

Backus, G. E. & Gilbert, F., 1970. Uniqueness in the inversion of inaccurate gross Earth data, *Phil. Trans. R. Soc. A*, **266**, 123–192.

Dziewonski, A. M. & Anderson, Don L., 1981. Preliminary Reference Earth Model, *Phys. Earth planet. Int.*, **25**, 297–356.

Gilbert, F., 1971. Ranking and winnowing gross earth data for inversion and resolution, *Geophys. J. R. astr. Soc.*, **23**, 125–128.

Masters, G., 1979. Observational constraints on the chemical and thermal structure of the earth's deep interior, *Geophys. J. R. astr. Soc.*, **57**, 507–534.

Nakanishi, I. & Anderson, Don L., 1984a. Aspherical heterogeneity of the mantle from phase velocities of mantle waves, *Nature*, **307**, 117–121.

Nakanishi, I. & Anderson, Don L., 1984b. Measurements of mantle wave velocities and inversion for lateral heterogeneity and anisotropy – II. Analysis by the single-station method, *Geophys. J. R. astr. Soc.*, **78**, 573–617.

Nataf, H. C., Nakanishi, I. & Anderson, Don L., 1984. Anisotropy and shear-velocity heterogeneities in the upper mantle, *Geophys. Res. Lett.*, **11**, 109–112.

Tanimoto, T. & Anderson, Don L., 1984. Mapping convection in the mantle, *Geophys. Res. Lett.*, **11**, 287–290.

Tanimoto, T. & Anderson, Don L., 1985. Lateral heterogeneity and azimuthal anisotropy of the upper mantle: Love and Rayleigh waves 100–250 sec., *J. geophys. Res.*, submitted.

Whaler, K. A., 1984. Fluid upwelling at the core–mantle boundary – resolvability from surface geomagnetic data, *Geophys. J. R. astr. Soc.*, **78**, 453–473.

Whaler, K. A. & Gubbins, D., 1981. Spherical harmonic analysis of the geomagnetic field: an example of a linear inverse problem, *Geophys. J. R. astr. Soc.*, **65**, 645–693.

Woodhouse, J. H. & Dziewonski, A. M., 1984. Mapping the upper mantle: three dimensional modelling of earth structure by inversion of seismic waveforms, *J. geophys. Res.*, **89**, 5953–5986.

Woodhouse, J. H. & Girnius, T. P., 1982. Surface waves and free oscillations in a regionalized earth model, *Geophys. J. R. astr. Soc.*, **68**, 653–673.